ORIGINAL ARTICLE

Performance of Galileo precise time and frequency transfer models using quad-frequency carrier phase observations

Pengfei Zhang[1,2,3] · Rui Tu[1,2,4] · Yuping Gao[1,2,3] · Rui Zhang[1,4] · Junqiang Han[1,4]

Abstract

GNSSs, such as Galileo and modernized GPS, BeiDou and GLONASS systems, offer new potential and challenges in precise time and frequency transfer using multi-frequency observations. We focus on the performance of Galileo time and frequency transfer using the E1, E5a, E5b and E5 observations. Dual-frequency, triple-frequency and quad-frequency models for precise time and frequency transfer with different Galileo observations are proposed. Four time and transfer links between international time laboratories are used to assess the performances of different models in terms of time link noise level and frequency stability indicators. The average RMS values of the smoothed residuals of the clock difference series are 0.033 ns, 0.033 ns and 0.034 ns for the dual-frequency, triple-frequency and quad-frequency models with four time links, respectively. With respect to frequency stability, the average stability values at 15,360 s are 9.51×10^{-15}, 9.46×10^{-15} and 9.37×10^{-15} for the dual-frequency, triple-frequency and quad-frequency models with four time links, respectively. Moreover, although biases among different models and receiver the inter-frequency exist, their characteristics are relatively stable. Generally, the dual-/triple-/quad-frequency models show similar performance for those time links, and the quad-frequency models can provide significant potential for switching among and unifying the three multi-frequency solutions, as well as further enhancing the redundancy and reliability compared to the current dual-frequency time transfer method.

Keywords Galileo · Precise time and frequency transfer · Quad-frequency observations · Precise point positioning

Introduction

Since the GPS has proved to be an effective spatial tool for the comparison of remote time and frequency standards, it has been the subject of increased focus in the time–frequency area. From the initial approach of common-view and all-in-view techniques (Allan and Weiss 1980; Defraigne and Petit 2003; Weiss et al. 2005; Petit and Jiang 2008), which use only pseudorange measurements, to the development of the carrier phase (CP) technique, which combines dual-frequency carrier phase observations (Ray and Senior 2005), the accuracy of GPS time transfer has undergone significant improvements (Defraigne and Bruyninx 2007), and it has therefore been integrated into standard data analysis algorithms for the computation of the international atomic time (TAI) since 2009.

In recent years, with the modernization of GPS and GLONASS and the development of BeiDou (BDS) and Galileo systems, research on the use of emerging GNSSs has been undertaken to guarantee the accuracy, redundancy and robustness of previous GPS-only time transfer (Defraigne and Baire 2011; Jiang and Lewandowski 2012a, b). The new-generation GNSS satellite transmits signals at more than two frequencies. The Block IIF satellites of GPS include three signals at L1 (1575.42 MHz), L2 (1227.60 MHz) and L5 (1176.45 MHz) (https://www.gps.gov/). The Chinese BDS was designed to provide three signals at B1 (1561.098 MHz), B2 (1207.14 MHz) and B3 (1268.52 MHz) (http://www.beidou.gov.cn).

✉ Rui Tu
turui-2004@126.com

1 National Time Service Center, Chinese Academy of Sciences, Xi'an 710600, China

2 University of Chinese Academy of Sciences, Beijing 100049, China

3 Key Laboratory of Time and Frequency Primary Standards, Chinese Academy of Sciences, Xi'an 710600, China

4 Key Laboratory of Precision Navigation and Timing Technology, Chinese Academy of Sciences, Xi'an 710600, China

Time and frequency transfer based on the BDS has been the subject of considerable interest, and its performance has been invested in depth. Huang and Defraigne (2016) use BDS for time transfer with the standard common GPS GLONASS time transfer standard (CGGTTS). Guang et al. (2018) analyzed the performance of BDS time and frequency transfer at the National Time Service Center (NTSC), and Liang et al. (2018) evaluated BDS time transfer over multiple intercontinental baselines as a UTC contribution. Using BDS triple-frequency observation is expected to improve the current BDS time transfer performance. Tu et al. (2018a, b) demonstrated that the BDS triple-frequency model can be applied for CP precise time and frequency transfer with accuracy and stability identical to that of the dual-frequency model. Moreover, the European Galileo system is capable of transmitting signals with low noise and superior multipath performance in the E5 frequency band (1191.795 MHz). In this frequency band, Galileo forms two sub-carriers, namely E5a (1176.45 MHz) and E5b (1207.14 MHz), spaced at 30.69 MHz. The potential of using Galileo E5 observation for time transfer has been well investigated using a single frequency or by forming dual-frequency observation with E1 (1575.42 MHz) measurements (Martínez-Belda et al. 2011, 2013; Zhang et al. 2019).

Conventionally, ionospheric-free (IF) combination with dual-frequency carrier phase and code measurements has been employed for P3 and L3 observations with the CP technique for time and frequency transfer (Petit and Defraigne 2016; Zhang et al. 2018). However, the availability of multi-frequency signals can provide significant opportunities for improving the performance. With additional frequencies, GNSS data processing, such as cycle slip detection, ambiguity resolution and phase multipath estimation from a single station, can be performed more effectively than with dual-frequency observations only (Simsky 2006; Dai et al. 2009; Zhang and Li 2016; Guo et al. 2016; Li et al. 2019). Various studies have focused on benefits in terms of positioning, such as relative positioning (Teunissen et al. 2002) and precise point positioning (PPP) (Elsobeiey 2015). Tegedor and Øvstedal (2014) demonstrate that the new L5 observation can increase robustness. Deo and El-Mowafy (2016) proposed two new PPP models that use triple-frequency data to accelerate the convergence of carrier phase float ambiguities. Considering that similar GNSS data processing strategies exist between positioning and time transfer, the multi-frequency data might be usefully applied in the area of time transfer.

Regarding time and frequency transfer, the BDS-2 triple-frequency model was proposed, and the results demonstrated accuracy and stability that were identical to those of dual-frequency CP models (Tu et al. 2018a). Moreover, the performance of the BDS-3 triple-frequency time transfer has been investigated (Su and Jin 2019). The number of BDS-3 satellites is quite limited at present, and thus, the triple-frequency contribution has not yet been effectively demonstrated. However, the Galileo system has a sufficient number of satellites, comprising 26 satellites: 4 in-orbit validation satellites and 22 full operational capability satellites (http://mgex.igs.org/IGS_MGEX_Status_GAL.php) at the end of 2018. Figure 1 presents the ground tracks of Galileo satellites available for time transfer on February 1, 2019. Although a huge potential exists for Galileo time and frequency transfer, particularly because of its superior E5 frequency, studies in recent years have focused only on dual-frequency observations and not on multi-frequency observations (Martínez-Belda et al. 2011, 2013; Zhang et al. 2019). With Galileo's superior E5 signal and its sub-carriers

Fig. 1 Ground tracks of the Galileo system as of February 1, 2019
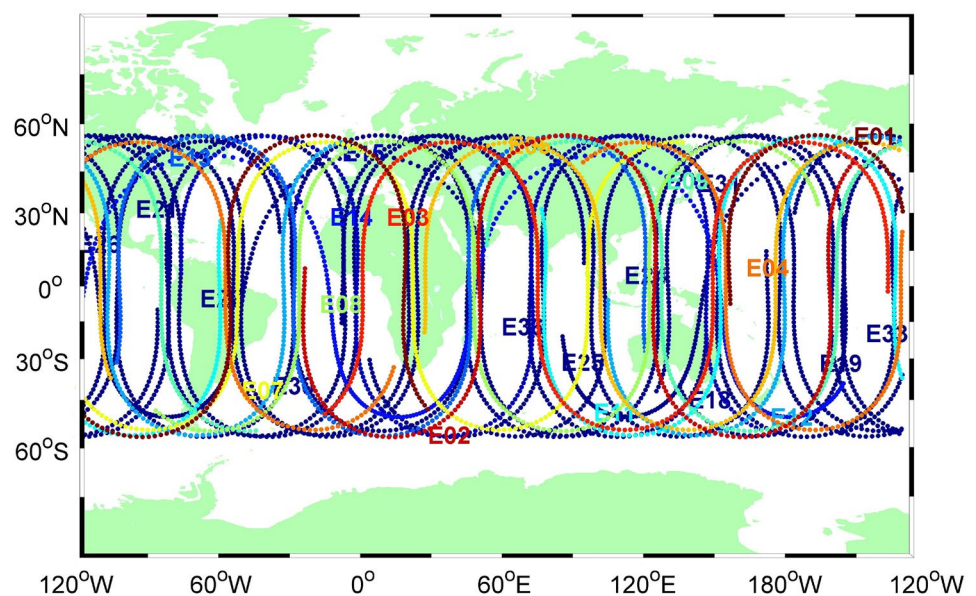
(E5a and E5b) and E1 observations, additional combination options are available, and the redundancy of observations is significantly increased compared to that of current dual-frequency Galileo time transfer. The results of previous studies on multi-frequency positioning have indicated that GNSS observations suffer from serious inter-frequency clock bias (Li et al. 2017). Therefore, how to handle these new biases in practical time transfer applications using multi-frequency observation is another major research topic.

In this study, mathematical models for dual-frequency, triple-frequency and quad-frequency Galileo CP time and frequency transfer are developed. Experiments were performed on four time links with observations from international time laboratories to assess the performance of the models. We begin with a brief description of mathematical models of the Galileo time and frequency transfer with dual-frequency, triple-frequency and quad-frequency observations. Then, the experimental design and data processing strategy for assessing the performance of the models are discussed. The results and discussion are presented. Finally, the summary and conclusions are given.

General observation model of the CP time and frequency transfer technique

The observation equations for the code P and carrier phase L at different frequencies can be generally expressed as follows (Leick et al. 2015; Li et al. 2015; Petit and Defraigne 2016):

$$P_{r,n}^s = \rho_r^s + c \cdot \left(dt_r - dt^s\right) + I_{r,n}^s + T_r^s + c \cdot t_d + e_{r,n}^s \tag{1}$$

$$L_{r,n}^s = \rho_r^s + c \cdot (dt_r - dt^s) - I_{r,n}^s + T_r^s + N_{r,n}^s + \varepsilon_{r,n}^s \tag{2}$$

where the indices s, r and n represent the satellite, receiver and frequency identifiers, respectively. The symbol ρ_r^s denotes the geometric distance between the satellite and receiver, c is the speed of light in vacuum, dt_r and dt^s denote the receiver and satellite clock offsets, respectively, $I_{r,n}^s$ is the slant ionosphere delay for the corresponding frequency, T_r^s denotes the tropospheric delay, t_d is the instrumental code delay, $N_{r,n}^s$ is the integer ambiguity of the frequency n, and $e_{r,n}^s$ and $\varepsilon_{r,n}^s$ are the sum of the noise and multipath error for the code and carrier phase observations, respectively. It is important to note that the phase center offset and variation, tidal loading, ocean tides, phase windup and relativistic delay must be corrected in existing models, even though the associated terms do not explicitly appear in (1) or (2).

For the time and frequency transfer, the receiver clock offset dt_r is of interest as an unknown parameter, which denotes the clock difference between the Galileo system timescale (GST) and the time and frequency reference. When the hardware delays caused by the receiver, antenna

and cables have been calibrated (Rovera et al. 2014a, b), the transfer operation between two remote time and frequency references (namely A and B) can be realized. Then, the formula can be expressed as follows:

$$T(A) - T(B) = (dt_r(A) - GST) - (dt_r(B) - GST) = dt_r(A) - dt_r(B) \tag{3}$$

The code observation, which directly measures the time information, and the carrier phase observation, which offers the advantage of low noise levels, are used to achieve high performance of the receiver clock. This is known as the CP technique and is the same as the PPP technique in geodesy. The precise satellite orbit and clock products obtained from the IGS are used to control the errors from the satellite orbit and clock. The tropospheric delay T_r^s is usually expressed as the sum of the dry and wet components, which can be expressed by their zenith delays and corresponding mapping functions. In general, the dry component is effectively corrected by its empirical model, while the wet component is set as an unknown parameter for estimation. The first order of the ionospheric delay in the CP technique can be eliminated by forming the IF combination of the pseudorange and carrier phase observations, which is used extensively in the area of precise time and frequency transfer. Regarding the four frequencies of the Galileo data, additional IF combination options are available in precise time and frequency transfer.

Dual-frequency CP models

The traditional CP technique using the IF model, which can eliminate the ionospheric delay to the first order, has been extensively applied in dual-frequency observation. For the pseudorange and carrier phase observations, the mathematical models of the CP technique can be formed as follows:

$$\begin{cases} P_{r,mn}^s = a_m P_{r,m}^s + a_n P_{r,n}^s = \rho + c \cdot \left(dt_{r,mn} - dt^s\right) + T_r^s + e_{r,mn}^s \\ L_{r,mn}^s = a_m L_{r,m}^s + a_n L_{r,n}^s = \rho + c \cdot \left(dt_{r,mn} - dt^s\right) + T_r^s + N_{r,mn}^s + \varepsilon_{r,mn}^s \end{cases} \tag{4}$$

where the indices m and n represent the frequency index. For the four Galileo frequencies (E1, E5a, E5b and E5), six independent IF combinations can be formed for the coefficients of the IF dual-frequency combination. Because the noise amplification factors in the E5a/E5b, E5a/E5 and E5b/E5 IF combinations are substantially larger than those of the other three IF combinations, these are inappropriate to apply to CP time and frequency transfer. Therefore, the mathematical model of the CP technique using dual-frequency measurements (E1/E5a, E1/E5b and E1/E5) can be formed according to (4) in the Galileo time and frequency transfer.

However, so-called differential code biases (DCBs) exist among the code observations at different frequencies because the signals at different frequencies undergo

varying time delays when propagating through the satellite and receiver hardware. Users can cancel the effect of satellite DCBs by using the E1/E5a observation directly with an IF combination and IGS precise clock product, because this conventional clock product contains the satellite DCB

Triple-frequency CP models

For Galileo, the general CP triple-frequency IF model among the four frequency observations for precise time and frequency transfer is as follows:

$$
\begin{cases}
P^s_{r,mnp} = b_m P^s_{r,m} + b_n P^s_{r,n} + b_p P^s_{r,p} = \rho + c \cdot (\mathrm{dt}_{r,mnp} - \mathrm{dt}^s) + T^s_r + \mathrm{DCB}^s_{mnp} + e^s_{r,mnp} \\
L^s_{r,mnp} = b_m L^s_{r,m} + b_n L^s_{r,n} + b_p L^s_{r,p} = \rho + c \cdot (\mathrm{dt}_{r,mnp} - \mathrm{dt}^s) + T^s_r + N^s_{r,mnp} + \varepsilon^s_{r,mnp}
\end{cases}
\tag{8}
$$

correction term of the E1/E5a IF combination. However, for the E1/E5b and E1/E5 combinations, the DCBs among different frequencies should be corrected for the Galileo CP models to remain compatible with the current precise clock product, which is formulated as follows:

$$
\mathrm{DCB}^s_{cp}(1,3) = \beta_{12} \cdot \mathrm{DCB}^s_{12} - \beta_{13} \mathrm{DCB}^s_{13} \tag{5}
$$

$$
\mathrm{DCB}^s_{cp}(1,4) = \beta_{12} \cdot \mathrm{DCB}^s_{12} - \beta_{14} \mathrm{DCB}^s_{14} \tag{6}
$$

where $\beta_{mn} = -\frac{f_n^2}{f_m^2 - f_n^2}$ and DCB^s_{mn} represent the satellite DCB parameters between the m and n frequencies, which can be obtained from the MGEX DCB products (ftp://cddis.gsfc.nasa.gov/pub/gps/products/mgex/dcb). The associated receiver DCBs will be lumped into the receiver clock offset with a constant and can be well calibrated. The dispersive coefficients and noises of the dual-frequency IF combinations are summarized in Table 1.

Therefore, the mathematical models (4) of the Galileo CP time and frequency transfer with dual-frequency observation can be transformed and linearized, and the estimated parameter vector X_{CP0} can be expressed as:

$$
X_{\mathrm{CP0}} = \left[x, y, z, \mathrm{dt}_{r,mn}, T_{\mathrm{wet}}, N^s_{r,mn} \right] \tag{7}
$$

where (x, y, z) are the station coordinate components and T_{wet} is the wet component.

Similarly, four sets of IF combinations can be formed among the E1, E5a, E5b and E5 signals, in which the noise amplification factor of the E5a/E5b/E5 IF combination is substantially larger than those of the other three IF combinations. Therefore, we pay more attention to the E1/E5a/E5b, E1/E5a/E5 and E1/E5b/E5 IF combinations in the Galileo triple-frequency CP technique for precise time and frequency transfer. The corresponding coefficients and noises of the triple-frequency CP model combinations are presented in Table 2. It can be observed the noises of the triple-frequency CP models are slightly smaller than those of the dual-frequency CP models.

The satellite DCBs should also be corrected according to the MGEX DCB products in the triple-frequency CP models. The corresponding correction terms for different triple-frequency CP models can be expressed as follows:

$$
\mathrm{DCB}^s_{cp1}(1,2,3) = (\beta_{12} - b_2) \cdot \mathrm{DCB}^s_{12} - b_3 \cdot \mathrm{DCB}^a_{13} \tag{9}
$$

$$
\mathrm{DCB}^s_{cp1}(1,2,4) = (\beta_{12} - b_2) \cdot \mathrm{DCB}^s_{12} - b_4 \cdot \mathrm{DCB}^s_{14} \tag{10}
$$

$$
\mathrm{DCB}^s_{cp1}(1,3,4) = \beta_{12} \cdot \mathrm{DCB}^s_{12} - b_3 \cdot \mathrm{DCB}^s_{13} - b_4 \cdot \mathrm{DCB}^s_{14} \tag{11}
$$

The values of the corresponding coefficient b_n are given in Table 2. It should be noted that the three pseudorange observations are combined for each of the triple-frequency CP

Table 1 Comparison of the three dual-frequency CP models for time and frequency transfer

Obs.	a_1	a_2	a_3	a_4	Noise	Satellite DCB correction
E1/E5a	2.261	− 1.261	0	0	2.588	0
E1/E5b	2.422	0	− 1.422	0	2.809	$\mathrm{DCB}^s_{cp}(1,3)$
E1/E5	2.338	0	0	− 1.338	2.694	$\mathrm{DCB}^s_{cp}(1,4)$

Table 2 Comparison of the three triple-frequency CP models for time and frequency transfer

Obs.	b_1	b_2	b_3	b_4	Noise	Satellite DCB correction
E1/E5a/E5b	2.315	− 0.836	− 0.479	0	2.508	$\mathrm{DCB}^s_{cp1}(1,2,3)$
E1/E5a/E5	2.293	− 0.734	0	− 0.559	2.472	$\mathrm{DCB}^s_{cp1}(1,2,4)$
E1/E5b/E5	2.373	0	− 0.593	− 0.780	2.567	$\mathrm{DCB}^s_{cp1}(1,3,4)$

models. The receiver hardware delay biases among different frequencies are absorbed by the receiver clock offset with a constant, which can be calibrated using the approach of the time link in the time and frequency transfer areas. Therefore, the parameters to be estimated in the triple-frequency CP model include the station coordinate components, receiver clock offset, tropospheric wet component and float ambiguities, which can be expressed as:

$$X_{\text{CP1}} = \left[x, y, z, \text{dt}_{\text{r},mnp}, T_{\text{wet}}, N^{\text{s}}_{\text{r},mnp}\right] \tag{12}$$

$$\begin{cases} P^{\text{s}}_{\text{r},15a} = c_1 P^{\text{s}}_{\text{r},1} + c_2 P^{\text{s}}_{\text{r},5a} = \rho + c \cdot \left(\text{dt}_{\text{r},15a} - \text{dt}^{\text{s}}\right) + T^{\text{s}}_{\text{r}} + e_{\text{r},15a} \\ L^{\text{s}}_{\text{r},15a} = c_1 L^{\text{s}}_{\text{r},1} + c_2 L^{\text{s}}_{\text{r},5a} = \rho + c \cdot \left(\text{dt}_{\text{r},15a} - \text{dt}^{\text{s}}\right) + T^{\text{s}}_{\text{r}} + N^{\text{s}}_{\text{r},15a} + \varepsilon^{\text{s}}_{\text{r},15a} \\ P^{\text{s}}_{\text{r},15b} = c_1 P^{\text{s}}_{\text{r},1} + c_3 P^{\text{s}}_{\text{r},5b} = \rho + c \cdot \left(\text{dt}_{\text{r},15a} - \text{dt}^{\text{s}}\right) + \text{IFB1}_{cp2} + \text{DCB}^{\text{s}}_{15b} + T^{\text{s}}_{\text{r}} + e_{\text{r},15b} \\ L^{\text{s}}_{\text{r},15b} = c_1 L^{\text{s}}_{\text{r},1} + c_3 L^{\text{s}}_{\text{r},5b} = \rho + c \cdot \left(\text{dt}_{\text{r},15a} - \text{dt}^{\text{s}}\right) + T^{\text{s}}_{\text{r}} + N^{\text{s}}_{\text{r},15b} + \varepsilon^{\text{s}}_{\text{r},15b} \\ P^{\text{s}}_{\text{r},15} = c_1 P^{\text{s}}_{\text{r},1} + c_4 P^{\text{s}}_{\text{r},5} = \rho + c \cdot \left(\text{dt}_{\text{r},15a} - \text{dt}^{\text{s}}\right) + \text{IFB2}_{cp2} + \text{DCB}^{\text{s}}_{15} + T^{\text{s}}_{\text{r}} + e_{\text{r},15} \\ L^{\text{s}}_{\text{r},15} = c_1 L^{\text{s}}_{\text{r},1} + c_4 L^{\text{s}}_{\text{r},5} = \rho + c \cdot \left(\text{dt}_{\text{r},15a} - \text{dt}^{\text{s}}\right) + T^{\text{s}}_{\text{r}} + N^{\text{s}}_{\text{r},15} + \varepsilon^{\text{s}}_{\text{r},15} \end{cases} \tag{13}$$

where X_{CP1} denotes the estimable vector for the triple-frequency CP model.

Quad-frequency CP models

The Galileo quad-frequency CP model can be implemented in three ways: First, the measurements from four frequencies can be used in three dual-frequency CP models, as mentioned previously (E1/E5a, E1/E5b and E1/E5), which is defined as the "CP2" model. The second method involves combining two of the triple-frequency CP models to form the quad-frequency CP model (E1/E5a/E5b, E1/E5a/E5 and E1/E5b/E5), defined as the "CP3" model. Finally, the measurements from four frequencies can be used to establish the quad-frequency CP model directly with one combination (E1/E5a/E5b/E5), defined as the "CP4" model in this study.

CP2: three dual-frequency IF combinations

The CP2 model for the Galileo quad-frequency time and frequency transfer is implemented by combining the three dual-frequency CP models. However, the parameters of the receiver clock offset are different in the individual

dual-frequency CP models since they assimilate different receiver code biases. In the individual dual-frequency CP model, these receiver code biases can be calibrated together with other hardware delays at remote stations and thus do not need to be considered in the mathematical model. However, to account for the situation of the CP2 model, the additional parameters of inter-frequency bias (IFB) are introduced into the E1/E5b and E1/E5 code combinations to maintain compatibility among the three dual-frequency CP models. Therefore, the formula for the CP2 model can be written as follows:

where the c values are the coefficients of the quad-frequency CP model and where IFB_{15b} and IFB_{15} denote the IFB parameters between the E1/E5b, E1/E5 and E1/E5a code combinations. Therefore, the parameters to be estimated in the quad-frequency CP model include the station coordinates, receiver clock offset, IFB parameters, tropospheric wet component and float ambiguities, listed as follows:

$$X_{\text{CP2}} = \left[x, y, z, \text{dt}_{\text{r},15a}, \text{IFB1}_{cp2}, \text{IFB2}_{cp2}, T_{\text{wet}}, N^{\text{s}}_{\text{r},15a}, N^{\text{s}}_{\text{r},15b}, N^{\text{s}}_{\text{r},15}\right] \tag{14}$$

where X_{CP2} denotes the estimable vector for the quad-frequency CP model using three dual-frequency IF combinations.

CP3: two triple-frequency IF combinations

Unlike the quad-frequency CP model based on CP2, which has only one combination, the quad-frequency CP model based on CP3 can be implemented by combining two triple-frequency CP models among E1/E5a/E5b, E1/E5a/E5 and E1/E5b/E5. Similarly, additional unknown IFB parameters are required to maintain compatibility between the two triple-frequency CP combinations. Therefore, the three quad-frequency CP models with two triple-frequency CP combinations can be formulated as follows:

$$\begin{cases} P^{\text{s}}_{\text{r},15a5b} = c_1 P^{\text{s}}_{\text{r},1} + c_2 P^{\text{s}}_{\text{r},5a} + c_3 P^{\text{s}}_{\text{r},5b} = \rho + c \cdot \left(\text{dt}_{\text{r},15a5b} - \text{dt}^{\text{s}}\right) + \text{DCB}^{\text{s}}_{15a5b} + T^{\text{s}}_{\text{r}} + e_{\text{r},15a5b} \\ L^{\text{s}}_{\text{r},15a5b} = c_1 L^{\text{s}}_{\text{r},1} + c_2 L^{\text{s}}_{\text{r},5a} + c_3 L^{\text{s}}_{\text{r},5b} = \rho + c \cdot \left(\text{dt}_{\text{r},15a5b} - \text{dt}^{\text{s}}\right) + T^{\text{s}}_{\text{r}} + N^{\text{s}}_{\text{r},15a5b} + \varepsilon^{\text{s}}_{\text{r},15a5b} \\ P^{\text{s}}_{\text{r},15a5} = c_1 P^{\text{s}}_{\text{r},1} + c_2 P^{\text{s}}_{\text{r},5a} + c_4 P^{\text{s}}_{\text{r},5} = \rho + c \cdot \left(\text{dt}_{\text{r},15a5b} - \text{dt}^{\text{s}}\right) + \text{IFB}_{15a5} + \text{DCB}^{\text{s}}_{15a5} + T^{\text{s}}_{\text{r}} + e_{\text{r},15a5} \\ L^{\text{s}}_{\text{r},15a5} = c_1 L^{\text{s}}_{\text{r},1} + c_2 L^{\text{s}}_{\text{r},5a} + c_4 L^{\text{s}}_{\text{r},5} = \rho + c \cdot \left(\text{dt}_{\text{r},15a5b} - \text{dt}^{\text{s}}\right) + T^{\text{s}}_{\text{r}} + N^{\text{s}}_{\text{r},15a5} + \varepsilon^{\text{s}}_{\text{r},15a5} \end{cases} \tag{15}$$

$$
\begin{cases}
P^s_{r,15a5b} = c_1 P^s_{r,1} + c_2 P^s_{r,5a} + c_3 P^s_{r,5b} = \rho + c \cdot \left(dt_{r,15a5b} - dt^s\right) + DCB^s_{15a5b} + T^s_r + e_{r,15a5b} \\
L^s_{r,15a5b} = c_1 L^s_{r,1} + c_2 L^s_{r,5a} + c_3 L^s_{r,5b} = \rho + c \cdot \left(dt_{r,15a5b} - dt^s\right) + T^s_r + N^s_{r,15a5b} + \varepsilon^s_{r,15a5b} \\
P^s_{r,15b5} = c_1 P^s_{r,1} + c_3 P^s_{r,5b} + c_4 P^s_{r,5} = \rho + c \cdot \left(dt_{r,15a5b} - dt^s\right) + IFB_{15b5} + DCB^s_{15b5} + T^s_r + e_{r,15b5} \\
L^s_{r,15b5} = c_1 L^s_{r,1} + c_3 L^s_{r,5b} + c_4 L^s_{r,5} = \rho + c \cdot \left(dt_{r,15a5b} - dt^s\right) + T^s_r + N^s_{r,15b5} + \varepsilon^s_{r,15b5}
\end{cases}
\tag{16}
$$

$$
\begin{cases}
P^s_{r,15a5} = c_1 P^s_{r,1} + c_2 P^s_{r,5a} + c_4 P^s_{r,5} = \rho + c \cdot \left(dt_{r,15a5} - dt^s\right) + DCB^s_{15a5} + T^s_r + e_{r,15a5} \\
L^s_{r,15a5} = c_1 L^s_{r,1} + c_2 L^s_{r,5a} + c_4 L^s_{r,5} = \rho + c \cdot \left(dt_{r,15a5} - dt^s\right) + T^s_r + N^s_{r,15a5} + \varepsilon^s_{r,15a5} \\
P^s_{r,15b5} = c_1 P^s_{r,1} + c_3 P^s_{r,5b} + c_4 P^s_{r,5} = \rho + c \cdot \left(dt_{r,15a5} - dt^s\right) + IFB_{15b5} + DCB^s_{15b5} + T^s_r + e_{r,15b5} \\
L^s_{r,15b5} = c_1 L^s_{r,1} + c_3 L^s_{r,5b} + c_4 L^s_{r,5} = \rho + c \cdot \left(dt_{r,15a5} - dt^s\right) + T^s_r + N^s_{r,15b5} + \varepsilon^s_{r,15b5}
\end{cases}
\tag{17}
$$

where the model combining E1/E5a/E5b and E1/E5a/E5 is defined as CP3-1, the model combining E1/E5a/E5b and E1/E5b/E5 is defined as CP3-2, and the model combining E1/E5a/E5 and E1/E5b/E5 is defined as CP3-3. Moreover, IFB_{15a5} and IFB_{15b5} denote the IFB parameters between the E1/E5a/E5, E1/E5b/E5 and E1/E5a/E5b code combinations. The IFB parameter between the E1/E5a/E5 and E1/E5b/E5 code combinations is symbolized as IFB_{15b5}. Thus, the unknown parameters for the quad-frequency CP model can be summarized as follows:

$$
X_{CP3-1} = \left[x, y, z, dt_{r,15a5b}, IFB_{cp3-1}, T_{wet}, N^s_{r,15a5b}, N^s_{r,15a5}\right]
\tag{18}
$$

$$
X_{CP3-2} = \left[x, y, z, dt_{r,15a5b}, IFB_{cp3-2}, T_{wet}, N^s_{r,15a5b}, N^s_{r,15b5}\right]
\tag{19}
$$

$$
X_{CP3-3} = \left[x, y, z, dt_{r,15a5}, IFB_{cp3-3}, T_{wet}, N^s_{r,15a5}, N^s_{r,15b5}\right]
\tag{20}
$$

where X_{CP3-1}, X_{CP3-2} and X_{CP3-3} denote the estimable vector for the quad-frequency CP model using two triple-frequency IF combinations.

CP4: single quad-frequency IF combination

The CP4 model for time and frequency transfer is formed with a single quad-frequency IF combination. Similar to the dual-frequency and triple-frequency models, the first order of the ionospheric delay cancels, and the geometric distance remains unchanged. Moreover, the amplification noise of the combination should be controlled within a certain range. Therefore, the coefficients for the quad-frequency IF combination are directly provided in Table 3. It should be noted that the four pseudorange measurements are combined within a single equation. The receiver hardware delay bias among the four frequency code observations is a constant that is ultimately incorporated in the receiver clock parameter. Since the hardware delay is calibrated in the time and frequency transfer, these biases do not have to be considered in the CP4 model. Thus, the equation for the CP4 model for the Galileo quad-frequency time and frequency transfer can be expressed as:

Table 3 Comparison of the five quad-frequency CP models for time and frequency transfer

Model	Obs.	c_1	c_2	c_3	c_4	Noise	Satellite DCB correction
CP2	E1/E5a	2.261	−1.261	0	0	2.589	0
	E1/E5b	2.422	0	−1.422	0	2.809	$DCB^s_{cp}(1,3)$
	E1/E5	2.338	0	0	−1.338	2.694	$DCB^s_{cp}(1,4)$
CP3-1	E1/E5a/E5b	2.315	−0.836	−0.479	0	2.508	$DCB^s_{cp1}(1,2,3)$
	E1/E5a/E5	2.293	−0.734	0	−0.559	2.472	$DCB^s_{cp1}(1,2,4)$
CP3-2	E1/E5a/E5b	2.315	−0.836	−0.479	0	2.508	$DCB^s_{cp1}(1,2,3)$
	E1/E5b/E5	2.373	0	−0.593	−0.78	2.567	$DCB^s_{cp1}(1,3,4)$
CP3-3	E1/E5a/E5	2.293	−0.734	0	−0.559	2.472	$DCB^s_{cp1}(1,2,4)$
	E1/E5b/E5	2.373	0	−0.593	−0.78	2.567	$DCB^s_{cp1}(1,3,4)$
CP4	E1/E5a/E5b/E5	2.317	−0.606	−0.274	−0.437	2.450	$DCB^s_{cp4}(1,2,3,4)$

$$\begin{cases} P^s_{r,mnpq} = c_m P^s_{r,m} + c_n P^s_{r,n} + c_p P^s_{r,p} + c_q P^s_{r,q} = \rho + c \cdot \left(dt_{r,mnpq} - dt^s \right) + T^s_r + DCB^s_{mnpq} + e^s_{r,mnpq} \\ L^s_{r,mnpq} = c_m L^s_{r,m} + c_n L^s_{r,n} + c_p L^s_{r,p} + c_q L^s_{r,q} = \rho + c \cdot \left(dt_{r,mnpq} - dt^s \right) + T^s_r + N^s_{r,mnpq} + \varepsilon^s_{r,mnpq} \end{cases} \tag{21}$$

The satellite DCB correction for the CP4 model can be expressed as:

$$DCB^s_{cp4}(1,2,3,4) = \left(\beta_{12} - b_2 \right) \cdot DCB^s_{12} - b_3 \cdot DCB^s_{13} - b_4 \cdot DCB^s_{14}. \tag{22}$$

Therefore, the parameters to be estimated in the quad-frequency CP model using a single quad-frequency IF combination include the station coordinates, receiver clock offset, tropospheric wet delay and float ambiguities, which can be listed as follows:

$$X_{CP4} = \left[x, y, z, dt_{r,15a5b5}, T_{wet}, N^s_{r,15a5b5} \right]. \tag{23}$$

where X_{CP4} denotes the estimable vector for the quad-frequency CP model using a single quad-frequency IF combination.

Table 3 summarizes the five quad-frequency Galileo CP models for precise time and frequency transfer, including the observations, coefficients for the individual models, noise amplification factors and satellite DCB corrections. It can be observed that the quad-frequency models of CP2 and CP3 are indirectly formed using dual-frequency and triple-frequency IF combinations, and the corresponding IFB parameters need to be introduced to maintain compatibility among different IF combinations. The quad-frequency model of CP4 is directly formed with code and CP measurements from the four frequencies. It can be observed that the noise amplification factor of CP4 is slightly smaller than those of the CP2 and CP3 models. Because the precise clock product is determined using the E1/E5a observation for Galileo, it contains the satellite DCB correction term of the E1/E5a IF combination, and hence, it does not need to be considered when using only the E1/E5a dual-frequency observation. The five quad-frequency CP models, all of which need to consider the DCB correction, and the corresponding formulas are summarized in Table 3.

Time and frequency transfer experiment

To evaluate Galileo time and frequency transfer with multi-frequency observations, five stations equipped with UTC (laboratory) time and frequency references were selected. The site names, GNSS receiver and antenna types, corresponding frequency standards and locations are summarized in Table 4. It should be noted that the receivers are all manufactured from Septentrio in Belgium; these receivers are widely used in time and frequency determination. Observations spanning from modified Julian dates (MJDs) 58,518–58,530 were collected as the experimental datasets for this study. Considering that station PT11, associated with the Physikalisch-Technische Bundesanstalt (PTB), is usually set as the central station in practical work of time and frequency transfer, we used it as a reference station in the experiment. Therefore, time links were formed, denoted by UTC(Lab2)–UTC(Lab1) or Station1–Station2, referring to the basic quantity that is generally used to analyze the performance of time and frequency transfer. Table 5 summarizes the four time links of the experiment and the corresponding geodetic distances, which spanned from 454.9 to 6274.8 km.

To evaluate the performance of those models, we developed a new time and frequency transfer software package named precise time transfer solution (PTTSol), which also supports multi-frequency time and frequency transfer. During data processing, the precise orbit and clock products were taken from the IGS data analysis center GFZ, which

Table 5 Time links formed and corresponding geodetic distances

Time link	Geodetic distance (km)
BRUX–PT11	454.9
WAB2–PT11	635.3
ROAG–PT11	2182.5
USN7–PT11	6274.8

Table 4 Attributes of stations used in the experiment of time and frequency transfer

Site name	GNSS receiver	Antenna	Frequency standard	Location
PT11	POLARX4TR	LEIAR25.R4	UTC(PTB)	52.2°N, 10.4°E
BRUX	POLARX4TR	JAVRINGANT_DM	UTC(ORB)	50.8°N, 4.4°E
ROAG	POLARX5TR	LEIAR25.R4	UTC(ROA)	36.5°N, 6.5°W
USN7	POLARX5TR	TPSCR.G5	UTC(USNO)	38.9°N, 77.1°W
WAB2	POLARX5TR	SEPCHOKE_B3E6	UTC(CH)	46.9°N, 7.5°E

Table 6 Observation models and Galileo multi-frequency RINEX data processing strategies for time and frequency transfer

Item	Models and strategies
Observations	Galileo carrier phase and code observations
Signal selection	E1/E5a/E5b/E5
Satellite orbit and clock	Precise satellite products from GFZ
Satellite antenna phase center offset	Corrected using MGEX values (Rizos et al. 2013)
Ionosphere	Eliminated by different IF combinations
Tropospheric delay	Initial model + random walk process
Elevation cutoff	7°
Sampling rate	30 s
Observation weight	Elevation-dependent weight
Estimator	LSQ in sequential mode
Receiver clock offset	Estimated as white noise process
Receiver IFB	Dual-frequency/triple-frequency/CP4 models: absorbed in receiver clock offset
	CP2/CP4 model: estimated as constant
Phase windup effect	Model corrected (Wu et al. 1993)
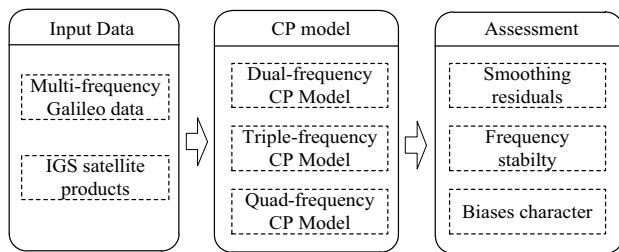
Fig. 2 Basic implementation of the multi-frequency Galileo time and frequency transfer experiment

can provide the Galileo orbit and clock products. Different IF combinations of the CP models were separately applied to eliminate the first-order ionospheric delay. The dry tropospheric delay was corrected by using the Saastamoinen model, while the residual zenith wet delay was estimated as a random walk process. A cutoff elevation angle of 7° and an elevation-dependent weighting approach were applied. Moreover, the receiver clock offset parameter was estimated as a white noise process. The receiver inter-frequency biases in the dual-frequency, triple-frequency and CP4 models were

Fig. 3 Number (up) of available Galileo satellites and TDOP (down) values from MJDs 58,518–58,530 at stations BURX (**a**), PT11 (**b**), ROAG (**c**), USN7 (**d**) and WAB2 (**e**)
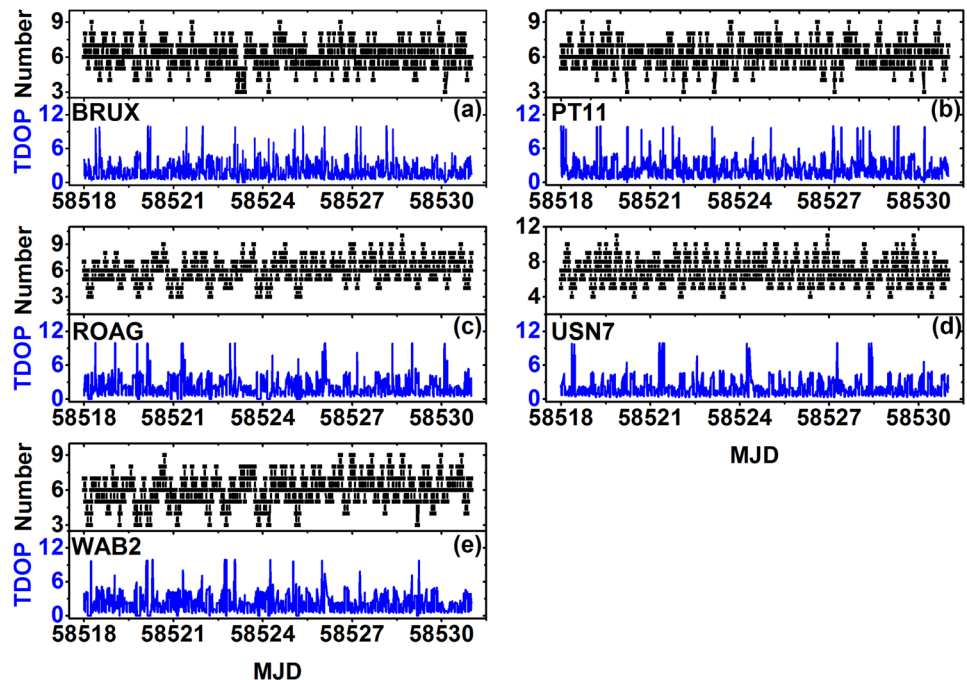
absorbed in the receiver clock offset, and this offset was estimated as constant in the CP2/CP4 model. Moreover, the phase windup effects were considered (Wu et al. 1993).

Table 6 summarizes the Galileo multi-frequency observation models and data processing strategies employed. Figure 2 shows the implementation of the experiments. The Galileo quad-frequency data collected at the stations and the IGS satellite products are the input data. Three kinds of multi-frequency CP models (dual-, triple- and quad-) are employed to achieve precise time transfer between time links. The performance of the multi-frequency models on different time links is assessed in terms of the smoothing residuals, frequency stability and bias character.

Results and discussion

For precise time and frequency transfer, the number of available satellites at a station and the time dilution of precision (TDOP) are key issues to be addressed prior to verifying the multi-frequency time and frequency transfer models. The fact that two external time and frequency references were individually installed at the two ends for the one time link and were running in real time during the experimental period affected the performance evaluation for different time transfer cases. Therefore, the root mean square (RMS) value of the smoothed residuals (Harmegnies et al. 2013) was used in this study; the RMS reflects the noise level of the time transfer link. Furthermore, the frequency stability of the time link is a crucial indicator of time and frequency transfer. Given

Table 7 Mean and STD values of the two model biases at different links

Time link	Bias1-dual		Bias2-dual	
	Mean (ns)	STD (ns)	Mean (ns)	STD (ns)
BRUX–PT11	2.732	0.065	1.648	0.035
ROAG–PT11	−6.759	0.030	−4.927	0.018
USN7–PT11	−4.811	0.066	−4.295	0.019
WAB2–PT11	−3.609	0.028	−2.281	0.014

that the Allan deviation (ADEV) (Jiang and Lewandowski 2012a, b) is a measure of the fractional frequency fluctuation and offers the advantage of convergence, it is the most commonly used time-domain measure of frequency stability. Therefore, the RMS and ADEV indicators were assessed for different multi-frequency CP models. Moreover, the IFBs were analyzed in the quad-frequency CP model.

Figure 3 illustrates the number of available Galileo satellites and TDOP values during the entire experiential period. The increase in the number of Galileo satellites offers significant opportunities for precise time and frequency transfer. For the 7° elevation cutoff, approximately 4–8 satellites could be observed at BRUX in most epochs, and the averaged value was 6.18. The average numbers of available satellites were 6.25 for PT11, 5.93 for ROAG, 6.79 for USN7 and 5.83 for WAB2. The average TDOP values were 1.98, 2.17, 2.13, 1.88 and 2.22 for BRUX, PT11, ROAG, USN7 and WAB2, respectively.

Fig. 4 Clock difference series of the three dual-frequency time transfer in nanoseconds from MJDs 58,518–58,530 at time links BRUX–PT11 (**a**), ROAG–PT11 (**b**), USN7–PT11 (**c**) and WAB2–PT11 (**d**)
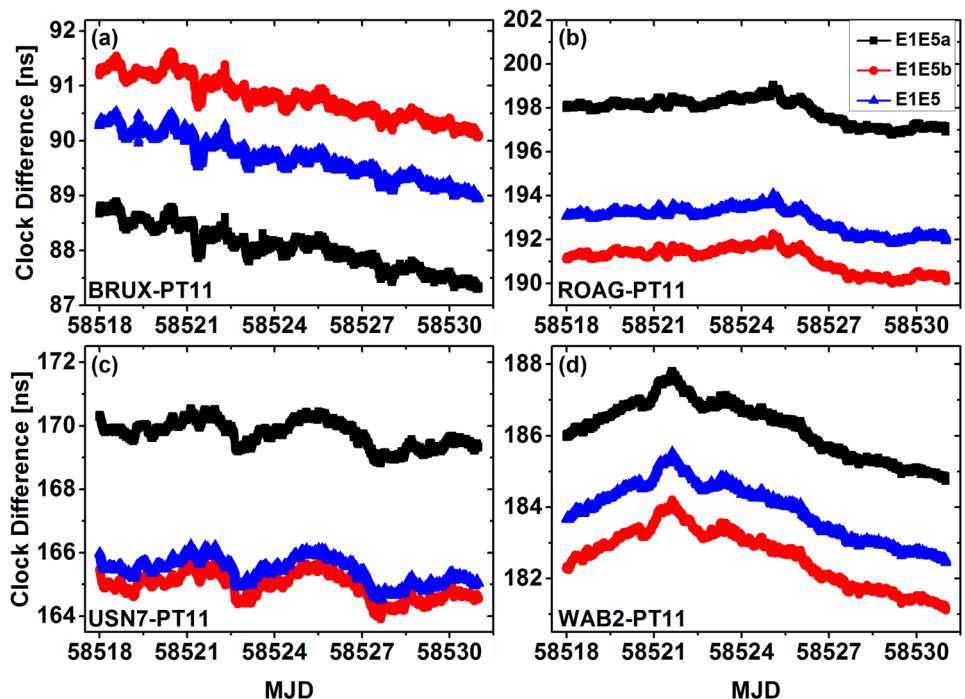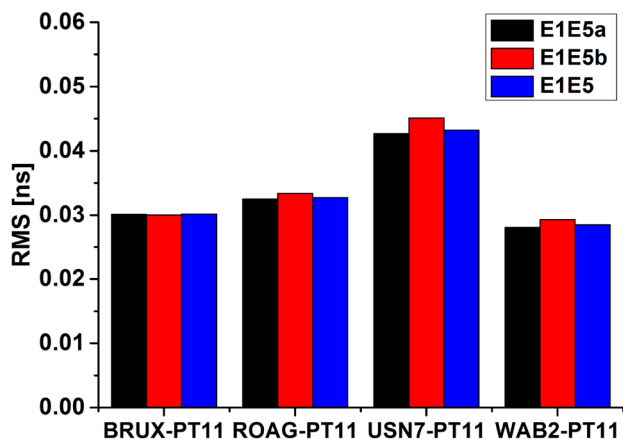
Fig. 5 RMS of smoothed residuals for the clock difference series derived by the three dual-frequency models from MJDs 58,518–58,530 at four time links

Dual frequency

Figure 4 presents the time transfer results for the three dual-frequency models in the four time links. The vertical axis (clock difference) represents the difference between the two receiver clock offsets at the two ends of the time link, which could be determined according to (3). It should be noted that the variations in the time transfer values agreed well for each solution. Moreover, clear biases existed among the solutions from the three different dual-frequency CP models, the reason for which is mainly the receiver clock offset being

absorbed by different receiver DCBs as varying frequencies undergoing different time delays.

To assess the performance of the biases between different dual-frequency models during the experiment, we selected the clock difference from the E1/E5a model as a reference. Therefore, the bias between E1/E5b and E1/E5a was denoted by "Bias1-Dual," while that between E1/E5 and E1/E5a was denoted by "Bias2-Dual." The statistical information of individual bias series includes mean and standard deviation (STD) indicators, which are summarized in Table 7. It can be noted that, although the two biases at the four time links differed (the maximum mean value was -6.759 ns at ROAG-PT11 in "Bias1-Dual," while the minimum was 1.648 ns at BRUX-PT11 in "Bias2-Dual"), these values were stable during the experimental period. Moreover, the standard deviation (STD) of Bias2-Dual, having an average value of 0.022 ns, was generally better than that of Bias1-Dual, with an average value of 0.047 ns at the four different time links. This implies that the E5 observation was superior to the sub-carrier observation from E5b. Therefore, effective calibration techniques such as relative and absolute techniques (Rovera et al. 2014a, b) can be applied in practical time and frequency transfer, thereby increasing the effective redundancy results compared to the current only one dual-frequency model in practical time transfer work.

In this study, the RMS value of smoothed residuals for the raw clock difference series was employed to reflect the noise level of the time transfer results, which was obtained by comparing the smoothed clock difference series using a Kalman filter. Figure 5 presents the RMS values for the

Fig. 6 Comparison of ADEVs for the three dual-frequency models from MJDs 58,518–58,530 at time links BRUX–PT11 (**a**), ROAG–PT11 (**b**), USN7–PT11 (**c**) and WAB2–PT11 (**d**)
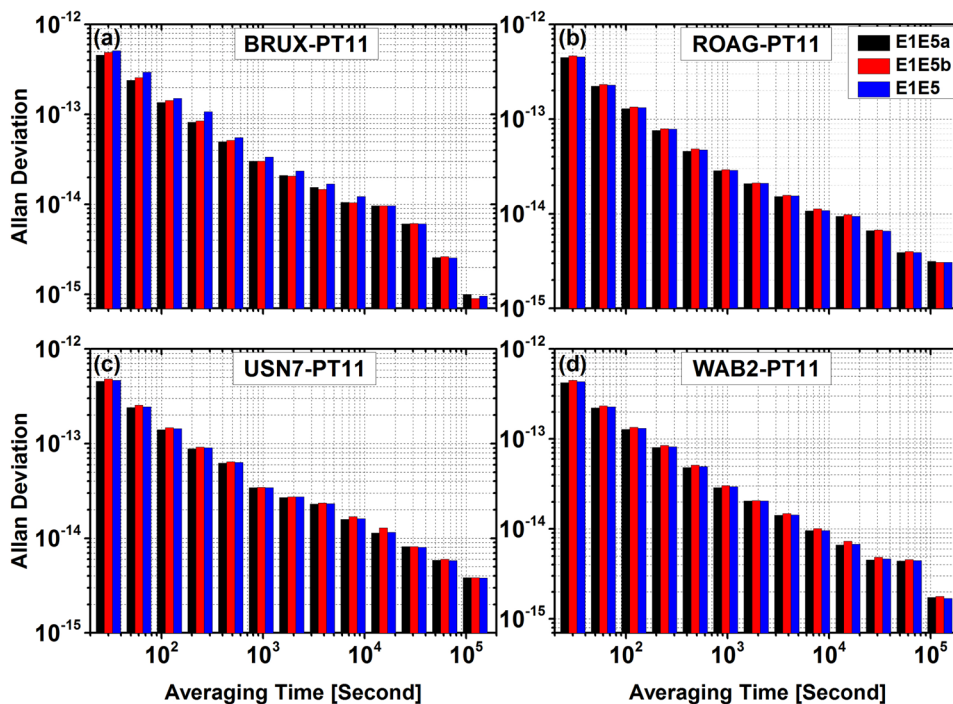
Fig. 7 Clock difference series of the three triple-frequency time transfer in nanoseconds from MJDs 58,518–58,530 at time links BRUX–PT11 (**a**), ROAG–PT11 (**b**), USN7–PT11 (**c**) and WAB2–PT11 (**d**)
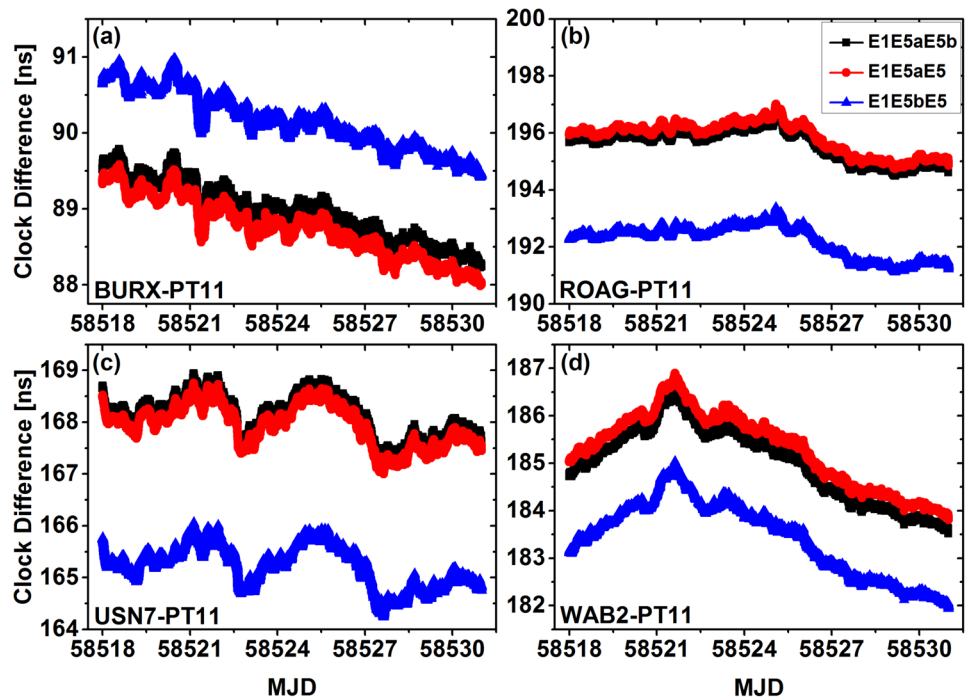
Table 8 Mean and STD values of the two triple-frequency model biases at different links

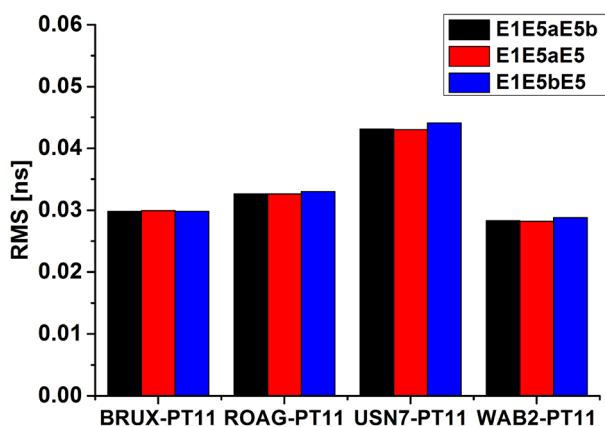| Time link	Bias1-triple		Bias2-triple	
	Mean (ns)	STD (ns)	Mean (ns)	STD (ns)
BRUX–PT11	−0.222	0.010	1.193	0.027
ROAG–PT11	0.254	0.006	−3.365	0.014
USN7–PT11	−0.179	0.008	−2.897	0.027
WAB2–PT11	0.299	0.005	−1.569	0.011

Fig. 8 RMS of smoothed residuals for the clock difference series derived by the three triple-frequency models from MJDs 58,518–58,530 at four time links

four time links. It can be noted that the RMS values were generally similar for the three dual-frequency models at the four time links. The average value was 0.033 ns for the E1/E5a solution, 0.033 ns for the E1/E5b solution and 0.034 ns for the E1/E5 solution. The E1/E5b solution was slightly inferior to the E1/E5a and E1/E5 solutions.

Figure 6 presents the ADEVs for the three dual-frequency modes at the four time links. To clearly show the difference between the three dual-frequency models, the ADEVs were drawn as column side by side. The frequency stabilities were also generally similar for the three dual-frequency models, regardless of the averaging time interval. The average stability values at 15,360 s for the four time links exceeded 9.27×10^{-15} for the E1/E5a solution, 9.92×10^{-15} for the E1/E5b solution and 9.35×10^{-15} for the E1/E5 solution.

Triple frequency

As discussed previously, three triple-frequency CP models were also implemented for the Galileo time and frequency transfer. Figure 7 illustrates the time transfer results of the three triple-frequency models at the four time links. The variation trends of the three different cases are generally identical, all reflecting the characteristics of the two external time and frequency references for one time link. Moreover, biases also existed among these three clock difference series. The bias between E1/E5a/E5 and E1/E5a/E5b is denoted by "Bias1-Triple," while that between E1/E5a/E5 and E1/E5b/

Fig. 9 Comparison of ADEVs for the three triple-frequency models from MJDs 58,518–58,530 at time links BRUX–PT11 (**a**), ROAG–PT11 (**b**), USN7–PT11 (**c**) and WAB2–PT11 (**d**)
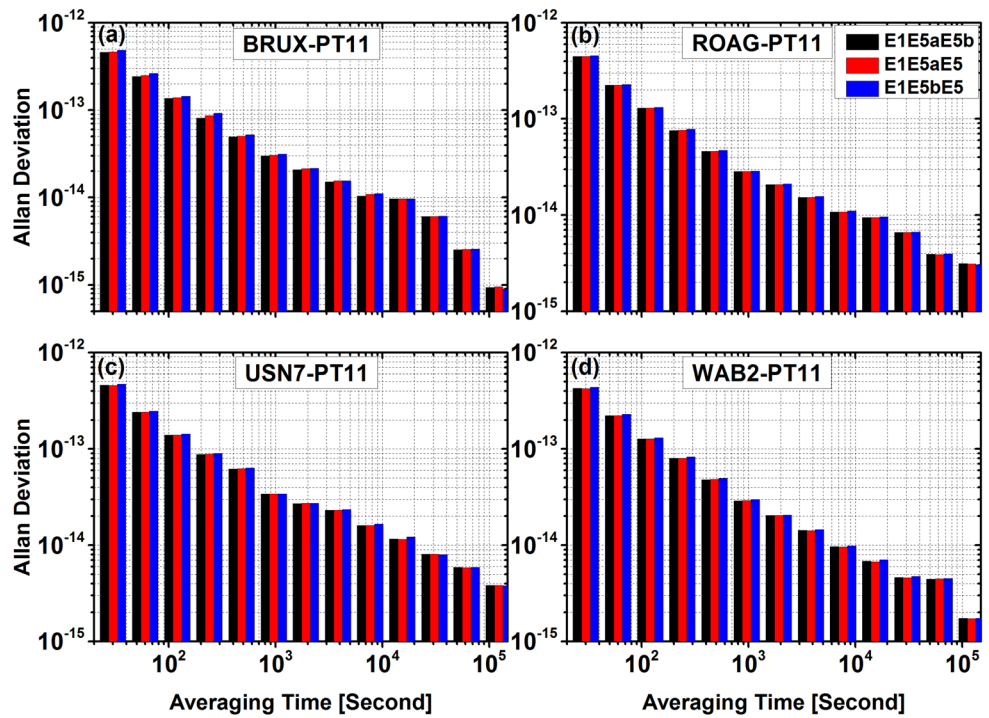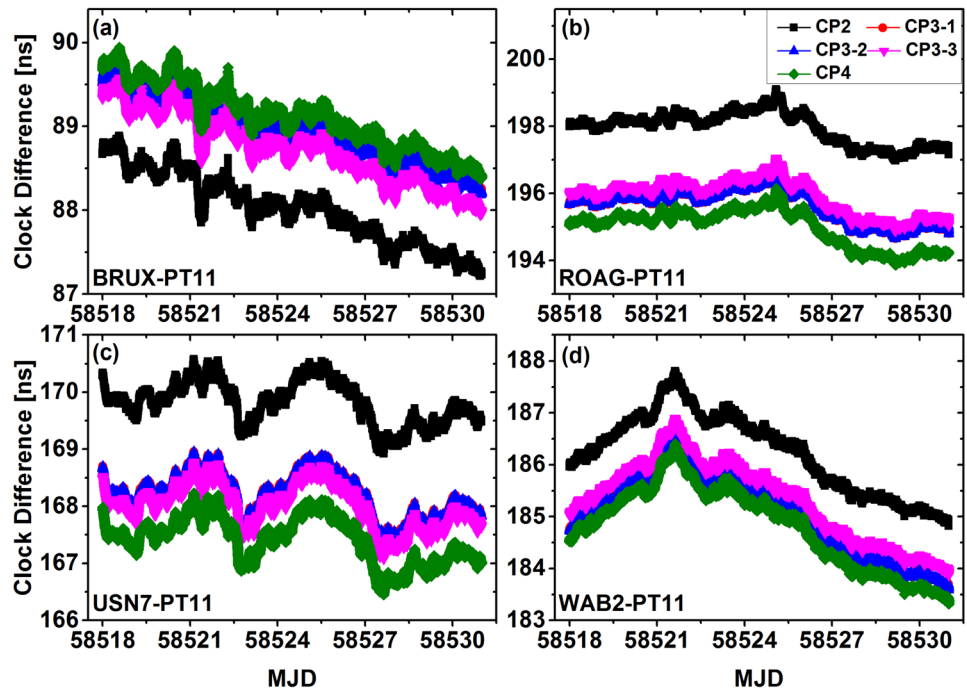
Fig. 10 Clock difference series of quad-frequency time transfer in nanoseconds from MJDs 58,518–58,530 at time links BRUX–PT11 (**a**), ROAG–PT11 (**b**), USN7–PT11 (**c**) and WAB2–PT11 (**d**)

E5 is denoted as "Bias2-Triple." Table 8 summarizes the statistical results for the biases. Although biases of different values are exhibited among the three triple-frequency models, i.e., the maximum mean value is −3.365 ns at ROAG-PT11 in "Bias2-Triple," while the minimum is −0.179 ns at BRUX-PT11 in "Bias1-Triple," the STDs are relatively stable. The average STD is 0.007 ns for "Bias1-Triple" and

0.020 ns for "Bias2-Triple," which is far less than the STD of the corresponding clock difference series with an average value of 0.535 ns. Therefore, it meets the prerequisite for the time link calibration among the three triple-frequency CP models.

Figure 8 presents a comparison of the RMS values from the three triple-frequency CP models for the four

Table 9 Mean and STD values of the two triple-frequency model biases at different links

Time link	Bias1-quad		Bias2-quad		Bias3-quad		Bias4-quad	
	Mean (ns)	STD (ns)	Mean (ns)	STD (ns)	Mean (ns)	STD (ns)	Mean (ns)	STD (ns)
BRUX–PT11	− 1.107	0.037	− 0.148	0.013	− 0.169	0.017	− 0.391	0.023
ROAG–PT11	2.969	0.094	0.681	0.068	0.672	0.064	0.923	0.061
USN7–PT11	2.401	0.050	0.766	0.037	0.763	0.035	0.582	0.034
WAB2–PT11	1.430	0.039	0.232	0.026	0.218	0.025	0.513	0.025
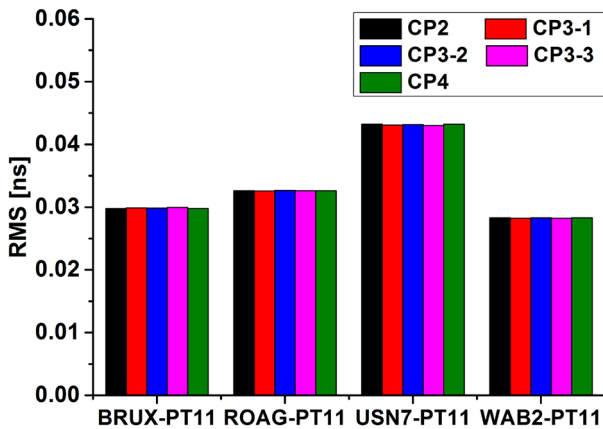
Fig. 11 RMS of smoothed residuals for the clock difference series derived by the five quad-frequency models at four time links

time links. The RMS values are also generally similar for different CP models. The average values at the four time links are 0.033 ns for the E1/E5a/E5b solution, 0.033 ns for the E1/E5a/E5 solution and 0.034 ns for the E1/E5b/E5 solution.

Furthermore, Fig. 9 presents a comparison of the frequency stability values for the three triple-frequency CP models. These values are generally identical for different solutions at the four time links. The average stability values at 15,360 s for the four time links surpassed 9.40×10^{-15} for the E1/E5a/E5b solution, 9.34×10^{-15} for the E1/E5a/E5 solution and 9.64×10^{-15} for the E1/E5b/E5 solution.

Quad frequency

There were four quad-frequency CP models for the time and frequency transfer, which were derived from the three dual-frequency CP combinations, the two triple-frequency CP models and the use of the observations from four frequencies directly. Figure 10 shows that the variations in the clock differences from the four solutions were generally identical, regardless of the time links, all representing the characteristics of the two time and frequency references during the experimental period. Moreover, the solutions

Fig. 12 Comparison of ADEVs for the four quad-frequency models from MJDs 58,518–58,530 at time links BRUX–PT11 (**a**), ROAG–PT11 (**b**), USN7–PT11 (**c**) and WAB2–PT11 (**d**)
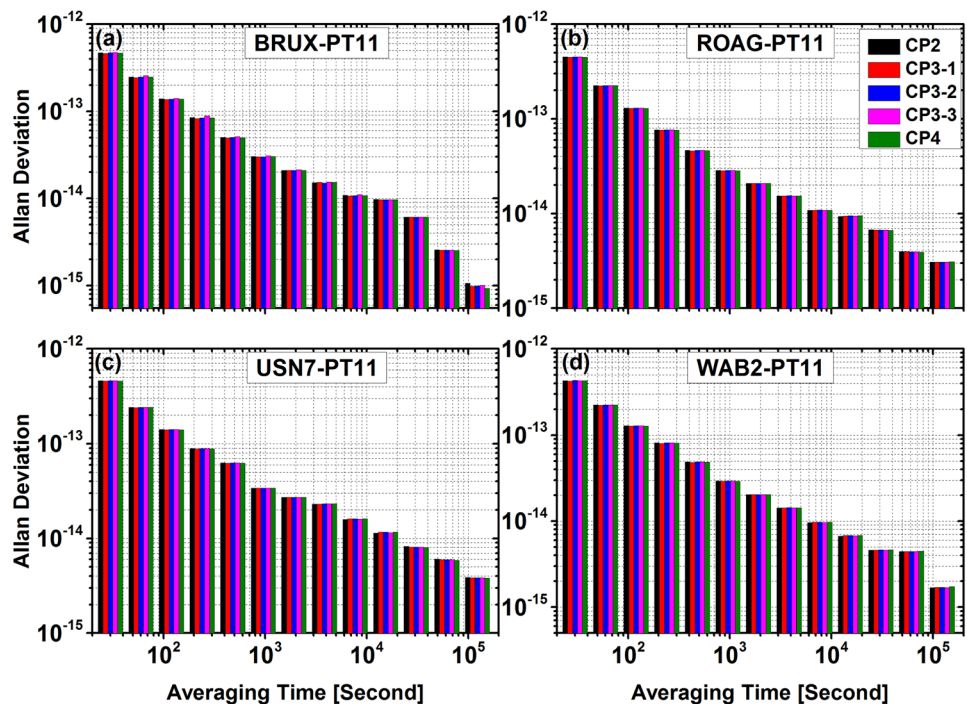
Fig. 13 Comparison of ADEVs for the dual (E1/E5a), triple (E1/E5a/E5b), and quad (E1/E5a/E5b/E5(CP4)) frequency models from MJDs 58,518–58,530 at time links BRUX–PT11 (**a**), ROAG–PT11 (**b**), USN7–PT11 (**c**) and WAB2–PT11 (**d**)
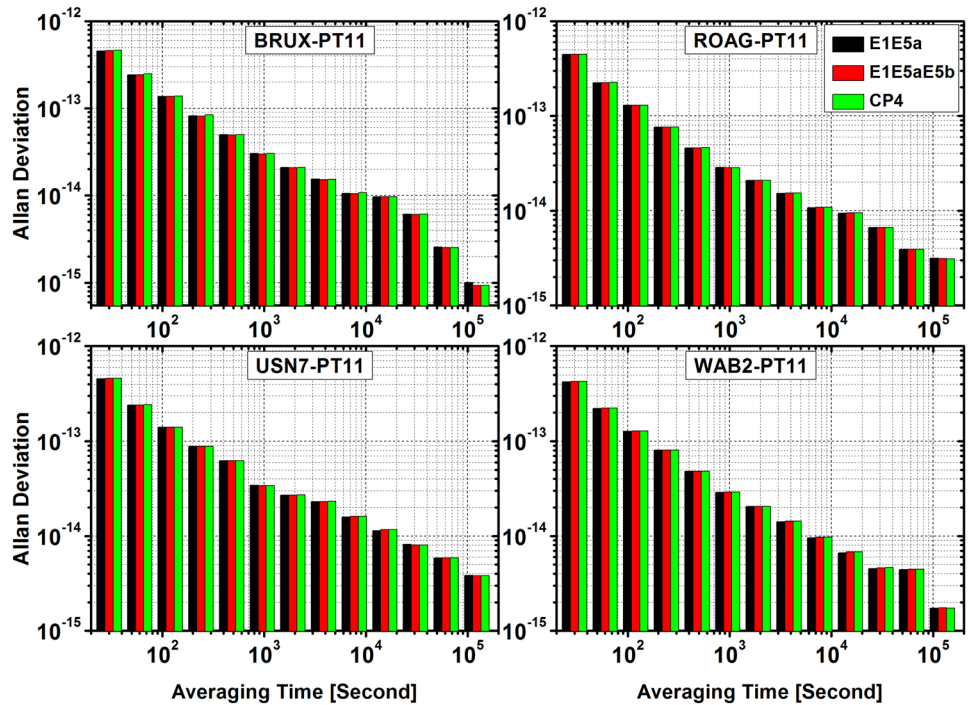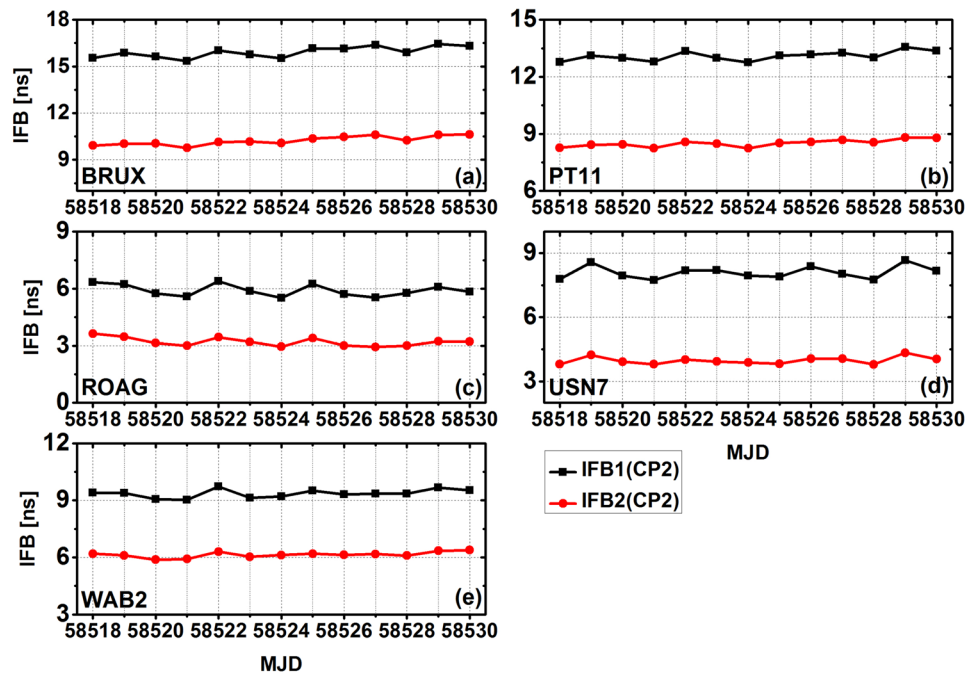

Fig. 14 Comparison of IFB series for the CP2 models in nanoseconds from MJDs 58,518–58,530 at stations BRUX (**a**), PT11 (**b**), ROAG (**c**), USN7 (**d**) and WAB2 (**c**)

from the CP3-1 and CP3-2 CP models are very similar because the receiver clock offsets in the two models all refer to the parameter from the E1/E5a/E5b combination. Similar to the other models, the biases among the four quad-frequency CP models were studied in depth. For convenience, we denote the biases between CP2 and CP4 as "Bias1-Quad," between CP3-1 and CP4 as "Bias2- Quad,"

between CP3-2 and CP4 as "Bias3-Quad" and between CP3-3 and CP4 as "Bias4-Quad." The statistical information is summarized in Table 9. The maximum mean value is 2.969 ns at ROAG-PT11 in "Bias2-Quad," while the minimum is -0.148 ns at BRUX-PT11 in "Bias2-Quad." The averaged STD value of the four biases at all modes is 0.041 ns, which is far less than the averaged STD of

Fig. 15 Comparison of IFB series for the CP3 models in nanoseconds from MJDs 58,518–58,530 at stations BRUX (**a**), PT11 (**b**), ROAG (**c**), USN7 (**d**) and WAB2 (**c**)
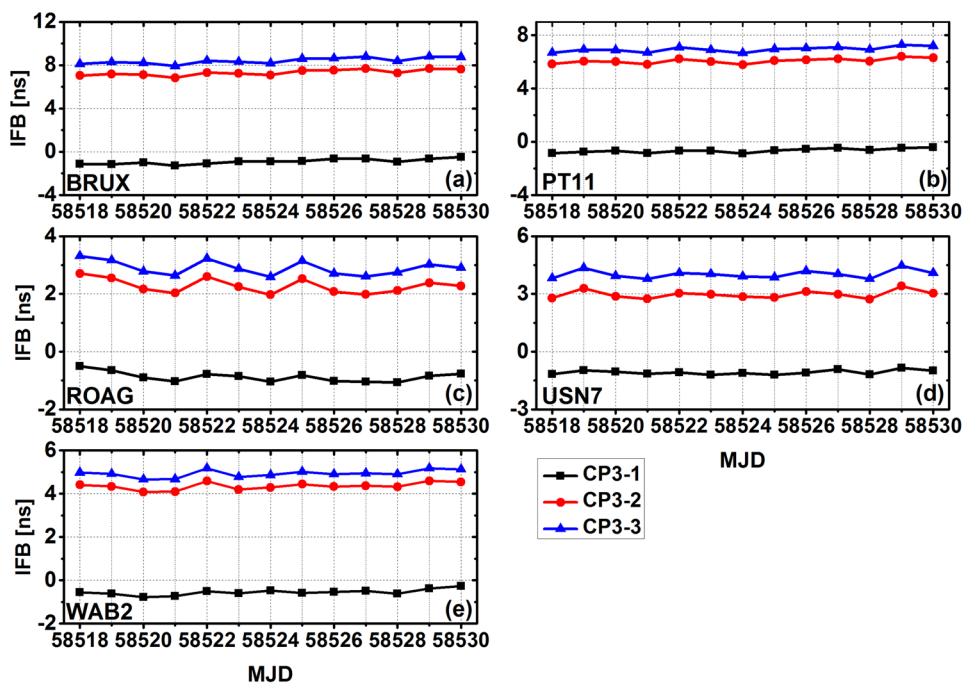
0.518 ns for the time transfer result. Therefore, these biases also exhibit relatively stable behavior during the entire experiment.

Figure 11 presents a comparison of the RMS values of the five quad-frequency CP models at the four time links. It can be noted that the RMS values are identical for different CP models. The average value at the four time links is better than 0.033 ns for the five CP models.

Figure 12 presents a comparison of the frequency stability values for the five quad-frequency CP models, which were generally identical for different solutions at the four time links. The average stability values at 15,360 s for the four time links surpassed 9.29×10^{-15} for CP2, 9.40×10^{-15} for CP3-1, 9.40×10^{-15} for CP3-2, 9.35×10^{-15} for CP3-3 and 9.41×10^{-15} for CP4.

To clearly compare the performance of the dual-, triple- and quad-frequency models, the corresponding ADEVs at the four time links are shown in Fig. 13. It can be noted that the three models are generally equivalent in frequency stability.

In the CP2 and CP3 models, additional unknown IFB parameters were introduced to maintain compatibility between different dual-frequency and triple-frequency IF combinations when indirectly forming the quad-frequency CP model. Figure 14 presents the two IFB value series for the CP2 model during the experimental period. It can be observed that, although the IFBs were estimated as constant for the daily solution, they still maintained high stability during the entire time transfer period. Additionally, the two types of IFB series exhibit strong agreement. The IFB values

of $IFB2_{cp2}$ are smaller than those of $IFB1_{cp2}$ at the five different stations. Furthermore, the averaged STD value of $IFB1_{cp2}$ is 0.287 ns and that of $IFB2_{cp2}$ is 0.203 ns for the 12 experimental days. Figure 15 presents the three IFB value series in the CP3 models, which are also highly stable even for 12 days at the five stations. The averaged STD value of $IFB1_{cp3}$ is 0.163 ns, that of $IFB2_{cp3}$ is 0.217 ns, and that of $IFB3_{cp3}$ is 0.220 ns.

Summary and conclusions

To exploit the potential of the Galileo multi-frequency code and CP observations in time and frequency transfer, we studied a multi-frequency model of Galileo precise time and frequency transfer based on the CP technique. The mathematical models for the dual frequency, triple frequency and quad frequency have been discussed and presented. Moreover, comprehensive numerical analyses were conducted to assess different multi-frequency CP models using datasets derived from five international time laboratories involving four time transfer links.

The results of the three dual-frequency CP models demonstrate that the variations in the clock difference series from the three solutions agree very well. The biases between the three models exhibited superior stability compared to the time transfer results during the entire experimental period. The average STD of those bias series reaches 0.047 ns and 0.022 ns for the three dual-frequency models. This provides significant potential for switching among the three

dual-frequency solutions and further enhances the redundancy of models compared to current time transfer. The RMS values of smoothed residuals are generally similar for the three dual-frequency models at the four time links. The average values are 0.133 ns for the E1/E5a solution, 0.138 ns for the E1/E5b solution and 0.135 ns for the E1/E5 solution. Additionally, the frequency stability values are generally similar for the three dual-frequency models, regardless of the averaging time interval. The average stability values at 15,360 s for the four time links reach 9.27×10^{-15} for the E1/E5a solution, 9.92×10^{-15} for the E1/E5b solution and 9.35×10^{-15} for the E1E5 solution. These results imply that the performance of the three dual-frequency CP models is generally identical, regardless of the noise level and frequency transfer.

The time and frequency transfer results of the three triple-frequency CP models also demonstrate strong agreement during the entire experimental period. Moreover, a statistical analysis of the biases among the three triple-frequency CP models was performed, and the average STD values are 0.007 ns and 0.020 ns, which are less than the 0.047 ns and 0.022 ns obtained for the three dual-frequency CP models. The major reason is that the additional observation used can provide a more robust time transfer result. Regarding the noise levels of the time transfer links, the RMS values are also generally similar for different CP models at the four time links, with 0.033 ns for the E1/E5a/E5b solution, 0.033 ns for the E1/E5a/E5 solution and 0.034 ns for the E1/E5b/E5 solution. Moreover, the frequency stability values are identical for the three solutions, even at different time intervals. The average stability values at 15,360 s at the four time links surpass 9.40×10^{-15} for the E1/E5a/E5b solution, 9.34×10^{-15} for the E1/E5a/E5 solution and 9.64×10^{-15} for the E1/E5b/E5 solution.

Five quad-frequency CP models were also developed for time and frequency transfer in this work, and the time and frequency transfer series results are also in strong agreement. The averaged STD value of the biases among the five CP models is 0.041 ns. The noise levels of time links are identical for different solutions, with average values superior to 0.033 ns at the four time links. Furthermore, the frequency stability values for the five quad-frequency CP models were generally identical for different solutions at the four time links, with average values of 9.29×10^{-15} for CP2, 9.40×10^{-15} for CP3-1, 9.40×10^{-15} for CP3-2, 9.35×10^{-15} for CP3-3 and 9.41×10^{-15} for CP4 at the 15,360-s time interval. Moreover, the characteristics of the receiver IFB are also analyzed. The averaged STD value of $IFB1_{cp2}$ is 0.287 ns and that of $IFB2_{cp2}$ is 0.203 ns for the 12 experimental days, while the averaged STD value of $IFB1_{cp3}$ is 0.163 ns, that of $IFB2_{cp3}$ is 0.217 ns, and that of $IFB3_{cp3}$ is 0.220 ns. These results imply that the IFB should be well estimated for the multi-frequency observation model for

time and frequency transfer. Moreover, the dual-frequency, triple-frequency and quad-frequency solutions were revealed to be generally equivalent, regardless of the noise level or frequency stability indicators for the time link. Fortunately, the biases between different CP models were relatively stable during the entire experimental period, which implies that these can be effectively predicted or calibrated in the area of time and frequency transfer and further enhance the performance of the current dual-frequency (E1/E5a) solution. At present, the multi-system and multi-frequency satellite navigation systems are undergoing rapid development. Further investigations into the application of time and frequency transfer will be valuable for enhancing and improving their performance.

References

Allan DW, Weiss MA (1980) Accurate time and frequency transfer during common-view of a GPS satellite. In: Proceedings of 34th annual frequency control symposium, USAERADCOM, Ft. Monmouth, WJ, May. pp 334–346

Dai Z, Knedlik S, Loffeld O (2009) Instantaneous triple-frequency GPS cycle-slip detection and repair. Int J Navig Obs. Article ID 407231. https://doi.org/10.1155/2009/407231

Defraigne P, Baire Q (2011) Combining GPS and GLONASS for time and frequency transfer. Adv Space Res 47(2):265–275

Defraigne P, Bruyninx C (2007) On the link between GPS pseudorange noise and day-boundary discontinuities in geodetic time transfer solutions. GPS Solut 11(4):239–249

Defraigne P, Petit G (2003) Time transfer to TAI using geodetic receivers. Metrologia 40(4):184–188

Deo M, El-Mowafy A (2016) Triple-frequency GNSS models for PPP with float ambiguity estimation: performance comparison using GPS. Surv Rev 50(360):249–261

Elsobeiey M (2015) Precise point positioning using triple-frequency GPS measurements. J Navig 68(3):480–492

Guang W, Dong S, Wu W, Zhang J, Yuan Y, Zhang S (2018) Progress of BeiDou time transfer at NTSC. Metrologia 55(2):175–187

Guo F, Zhang X, Wang J, Ren X (2016) Modeling and assessment of triple-frequency BDS precise point positioning. J Geod 90(11):1223–1235

Harmegnies A, Defraigne P, Petit G (2013) Combining GPS and GLONASS in all-in-view for time transfer. Metrologia 50(3):277–287

Huang W, Defraigne P (2016) BeiDou time transfer with the standard CGGTTS. IEEE Trans Ultrason Ferroelectr Freq Control 63(7):1005–1012. https://doi.org/10.1109/tuffc.2016.2517818

Jiang Z, Lewandowski W (2012a) Use of GLONASS for UTC time transfer. Metrologia 49(1):57–61

Jiang Z, Lewandowski W (2012b) Use of GLONASS for UTC time transfer. Metrologia 49:57–61

Leick A, Rapoport L, Tatarnikov D (2015) GPS satellite surveying, 4th edn. Wiley, New York

Li X, Ge M, Dai X, Ren X, Fritsche M, Wickert J, Schuh H (2015) Accuracy and reliability of multi-GNSS real-time precise positioning: GPS, GLONASS, BeiDou, and Galileo. J Geod 89(6):607–635

Li P, Zhang X, Li X, Liu J, Li X (2017) Characteristics of inter-frequency clock bias for Block IIF satellites and its effect on triple-frequency GPS precise point positioning. GPS Solut 21(2):811–822

Li X, Li X, Liu G, Feng G, Yuan Y, Zhang K, Ren X (2019) Triple-frequency PPP ambiguity resolution with multi-constellation GNSS: BDS and Galileo. J Geod 93(8):1105–1122

Liang K, Arias F, Petit G, Jiang Z, Tisserand L, Wang Y, Yang Z, Zhang A (2018) Evaluation of BeiDou time transfer over multiple inter-continental baselines towards UTC contribution. Metrologia 55(4):513–525

Martínez-Belda MC, Defraigne P, Baire Q, Aerts W (2011) Single-frequency time and frequency transfer with Galileo E5. In: Joint conference of the IEEE international frequency control and the european frequency and time forum (FCS) proceedings, San Francisco, CA, USA, 2011, pp 1–6. https://doi.org/10.1109/FCS.2011.5977741

Martínez-Belda MC, Defraigne P, Bruyninx C (2013) On the potential of Galileo E5 for time transfer. IEEE Trans Ultrason Ferroelectr Freq Control 60(1):121–131. https://doi.org/10.1109/TUFFC.2013.2544

Petit G, Defraigne P (2016) The performance of GPS time and frequency transfer: comment on 'A detailed comparison of two continuous GPS carrier-phase time transfer techniques'. Metrologia 53(3):1003–1008

Petit G, Jiang Z (2008) GPS All in view time transfer for TAI computation. Metrologia 45(1):35–45

Ray J, Senior K (2005) Geodetic techniques for time and frequency comparisons using GPS phase and code measurements. Metrologia 42(4):215–232

Rizos C, Montenbruck O, Weber R, Neilan R, Hugentobler U (2013) The IGS MGEX Experiment as a milestone for a comprehensive multi-GNSS service. In: Proceedings of pacific PNT meeting 2013, Honolulu, USA, April 22–25, pp 1–7

Rovera GD, Torre JM, Sherwood R, Abgrall M, Courde C, Laas-Bourez M, Uhrich P (2014a) Link calibration against receiver calibration: an assessment of GPS time transfer uncertainties. Metrologia 51(5):476–490

Rovera GD, Torre JM, Sherwood R, Abgrall M, Courde C, Laas-Bourez M, Uhrich P (2014b) Link calibration against receiver calibration: an assessment of GPS time transfer uncertainties. Metrologia 51:476–490

Simsky A (2006) Three's the charm: triple-frequency combinations in future GNSS. Inside GNSS 1(5):38–41

Su K, Jin S (2019) Triple-frequency carrier phase precise time and frequency transfer models for BDS-3. GPS Solut 23:86. https://doi.org/10.1007/s10291-019-0879-2

Tegedor J, Øvstedal O (2014) Triple carrier precise point positioning (PPP) using GPS L5. Surv Rev 46(337):288–297. https://doi.org/10.1179/1752270613Y.0000000076

Teunissen PJG, Joosten P, Tiberius C (2002) A comparison of TCAR, CIR and LAMBDA GNSS ambiguity resolution. In: Proceedings of ION GPS, Portland, Oregon, September 24–27, pp 2799–2808

Tu R, Zhang P, Zhang R, Liu J, Lu X (2018a) Modeling and performance analysis of precise time transfer based on BDS triple-frequency un-combined observations. J Geod 93(6):837–847

Tu R, Zhang P, Zhang R, Liu J, Lu X (2018b) Modeling and assessment of precise time transfer by using beidou navigation satellite system triple-frequency signals. Sensors 18(4):1017. https://doi.org/10.3390/s18041017

Weiss MA, Petit G, Jiang Z. (2005) A comparison of GPS common-view time transfer to all-in-view. In: Proceedings of the 2005

IEEE international frequency control symposium and exposition, Vancouver, BC, Canada, 29–31 August

Wu J, Wu S, Hajj G, Bertiger W, Lichten S (1993) Effects of antenna orientation on GPS carrier phase. Manuscr Geod 18:91–98

Zhang X, Li P (2016) Benefits of the third frequency signal on cycle slip correction. GPS Solut 20(3):451–460

Zhang P, Tu R, Zhang R, Gao Y, Cai H (2018) Combining GPS, Bei-Dou, and Galileo satellite systems for time and frequency transfer based on carrier phase observations. Remote Sens 10(2):324. https://doi.org/10.3390/rs10020324

Zhang P, Tu R, Gao Y, Liu N, Zhang R (2019) Improving Galileo's carrier-phase time transfer based on prior constraint information. J Navig 72(1):121–139

Publisher's Note Springer Nature remains neutral with regard to jurisdictional claims in published maps and institutional affiliations.

Pengfei Zhang is an associate researcher in the National Time Service Center at the Chinese Academy of Sciences. His main research interests include PPP timing and GNSS tropospheric study.

Rui Tu is a professor at the National Time Service Center at the Chinese Academy of Sciences. He received his Ph.D. in 2014 at Germany Research Center for Geosciences (GFZ). His main research interests include GNSS PPP, RTK positioning and application in geosciences.

Yuping Gao is a professor at the National Time Service Center at the Chinese Academy of Sciences. His main research interests include GNSS and pulsar timing.

Rui Zhang is an associate researcher in the National Time Service Center at the Chinese Academy of Sciences. He received his Ph.D. in 2016 at Chang'an University. His main research interests include BDS orbit determination and precise positioning.

Junqiang Han is an associate researcher in the National Time Service Center at Chinese Academy of Sciences. He received his Ph.D. in 2018 at Chang'an University. His main research interests include GNSS RTK positioning.